https://doi.org/10.5194/cp-2020-27
Preprint. Discussion started: 6 March 2020

Climate of the Past
Discussions

Dynamics of primary productivity in the northeastern Bay of Bengal over the last 26,000 years

Xinquan Zhou[1], Stéphanie Duchamp-Alphonse[1], Masa Kageyama[2], Franck Bassinot[2], Luc Beaufort[3], Christophe Colin[1]

[1]Université Paris-Saclay, Géosciences Paris Sud, UMR 8148, CNRS, Rue du Belvédère, 91405 Orsay, France

[2]Laboratoire des Sciences du Climat et de l'Environnement, UMR 8112, CEA/CNRS/UVSQ, Université Paris-Saclay, Centre CEA-Saclay, Orme des Merisiers, 91191 Gif-sur-Yvette, France

[3]Centre de Recherche et d'Enseignement de Géosciences de l'Environnement, UMR 7330, CNRS/IRD/Aix-Marseille Université, Av. Louis Philibert, BP80, 13545, Aix-en-Provence, France

Correspondance to : Xinquan Zhou (xinquan.zhou@universite-paris-saclay.fr)

Abstract. At present, variations of primary productivity (PP) in the Bay of Bengal (BoB) are responding to salinity-related-stratification which is controlled by the Indian Summer Monsoon (ISM). The relationships between PP, ISM, and to a broader scale, North Atlantic climate rapid variability in the past, are not clearly understood. Here, we present a new record of PP based on the examination of coccolithophore assemblages in a 26,000 years sedimentary record, retrieved in the northeastern BoB (core MD77-176). Comparisons with published climate and monsoon records, as well as outputs from the transient climate simulation TraCE-21 and experiments run with the Earth System Model IPSL-CM5A-LR, including marine biogeochemical components, helped us interpret our PP records in the context of ISM and Atlantic Overturning Meridional Circulation (AMOC) changes. We demonstrate that PP is influenced by vertical stratification in the upper water column over the last 26,000 years (26 kyr BP). It is controlled by wind-driven mixing from 26 to 19 kyr BP, i.e., when dry climate conditions and reduced freshwater inputs occurred, and by salinity-related-stratification over the last 19 kyr BP (since the Last Glacial Maximum), i.e., when humid conditions prevailed. During the deglaciation, salinity and stratification are related to monsoon precipitation dynamics, which are chiefly forced by both, insolation and the strength of the AMOC. The collapse (recovery) of the AMOC during Heinrich Stadial 1 (Bølling Allerød) weakened (strengthened) ISM and diminished (increased) stratification, thus enhancing (subduing) productivity.

https://doi.org/10.5194/cp-2020-27
Preprint. Discussion started: 6 March 2020

1. Introduction

The climatology and oceanography of the South Asia and the North Indian Ocean are dominated by the Indian Monsoon, which is characterized by strong seasonal contrasts in wind and precipitation patterns (Shankar et al., 2002; Gadgil et al., 2003). The Indian Monsoon is a subsystem of the large-scale Asian Monsoon, which is paced by seasonal changes in insolation due to the obliquity of the Earth's axis and results from variations in the land-sea thermal contrast caused by differences of heat capacity of the continent and the ocean (Meehl, 1994, 1997; Webster, 1998; Wang et al., 2003). The North Indian Ocean is strongly influenced by the southwesterly winds blowing from the sea during the northern hemisphere summer season thus carrying large amounts of moisture. The eastern part of the North Indian Ocean, i.e., the Bay of Bengal (BoB) and the Andaman Sea (ADS), receives heavier annual precipitation than its western counterpart, i.e. the Arabian Sea (AS). This discrepancy together with differences in local evaporation result in hydrological and ecological differences between these two areas (e.g. Prasanna Kumar et al., 2002; Vinayachandran et al., 2002; Shenoi et al., 2002; Shi W et al., 2002; Dey and Singh, 2003; Rao and Sivakumar, 2003; Prasad, 2004; Currie et al., 2013).

A noteworthy characteristic of modern conditions prevailing in the North Indian Ocean is the low PP in the BoB and the ADS compared to the AS (Prasanna Kumar et al., 2002). Previous studies revealed that low annual PP in the BoB results from the important freshwater input by rivers and direct rainfall on the sea, which cause a strong stratification of the upper water column (Vinayachandran et al., 2002; Madhupratap et al., 2003; Gauns et al., 2005). In contrast, AS has a high PP which is mainly associated with wind driven mixing and upwelling (Schott, 1983; Veldhuis et al., 1997; Keen et al., 1997; Prasanna Kumar et al., 2001). Thus, the western and eastern parts of the North Indian Ocean are remarkable examples of tropical ocean dynamics, which is characterized by limited seasonal differences of SST, and for which seasonal and interannual changes in PP result chiefly from variations in the nutricline depth (i.e. variations in nutrient availability in the photic zone) controlled by dynamical processes such as wind-driven mixing/upwelling, and/or by salinity-related stratification of the upper seawater column in relation to local evaporation-precipitation balance and river runoff (e.g. Lévy et al., 2001; Vinayachandran et al., 2002; Chiba et al., 2004; Rao et al., 2011; van de Poll et al., 2013; Behara and Vinayachandran, 2016; Spiro Haeger and Mahadevan, 2018).

Past changes of PP at both orbital- and millennial-scales in the western and northern AS have been widely studied, and authors have interpreted PP variations as chiefly reflecting changes in the intensity of Indian Summer Monsoon (ISM) southwesterly winds (e.g. Schultz et al., 1998; Ivanova et al., 2003; Ivanochko et al., 2005; Singh et al., 2011). Proxy reconstructions and climate model simulations have also pointed out that the Indian Summer Monsoon precipitation is sensitive to both the slow orbital forcing and then fast changes of high-latitude processes

https://doi.org/10.5194/cp-2020-27
Preprint. Discussion started: 6 March 2020

such as the Atlantic meridional overturning circulation (AMOC) and the temperature fluctuations in the North Atlantic (e.g. Braconnot et al., 2007a, 2007b; Kageyama et al., 2013; Marzin et al., 2013; Contreras-Rosales et al., 2014). However, the relationship between PP and monsoon precipitation in the past has been given less attention due to the absence of high time-resolution PP record in the BoB and the ADS (Phillips et al., 2014; Li et al., 2019), which precludes our complete understanding of how monsoon climate changes impact tropical ocean ecology through different mechanisms and at different time-scales. To fill this gap, a reliable paleo-PP record is needed for the BoB/ADS. On the other hand, the PP record can also indicate the variability of Indian Monsoon strength.
Coccolithophores are marine calcifying phytoplankton organisms that constitute one of the most important "functional groups", responsible for primary production and export of carbonate particles (i.e. the coccoliths they produce) to the sedimentary reservoir. The coccoliths preserved in marine sediment are good study material for paleoenvironmental reconstructions. Particularly, *Florisphaera profunda* is a lower photic zone dweller and its relative abundance in marine coccolithophore assemblages obtained from the sediments has been successfully used to reconstruct past changes of the nutricline depth and PP (Molfino and McIntyre, 1990a, 1990b; Beaufort et al., 1997; Zhang et al., 2016; Hernández-Almeida et al., 2019).
In this study, we provide the first record of coccolith assemblage changes in the BoB. The relative abundance of *F. profunda* in the sediment core MD77-176 makes it possible to reconstruct at a high-temporal resolution, paleo-PP over the last 26 kyr BP in the northeastern BoB. The studied period covers a complete precession cycle and the last deglaciation. This time interval is characterized by rapid climate changes remotely controlled by north hemispheric high-latitude climate and disruptions of the AMOC (McManus et al., 2004; Clement and Peterson, 2008; Liu et al., 2009; Wolff et al., 2010; Clark et al., 2012). In addition, we used the outputs of transient climate simulations run with the Community Climate System Model version 3 (CCSM3) (He et al., 2008; Collins et al., 2006a), and paleoclimate experiments run with the "Institut Pierre Simon Laplace" Earth System Model version 5 (IPSL-CM5A-LR) (Dufresne et al., 2013), in which marine biogeochemistry is represented, to analyze our PP results in terms of local evolution of upper seawater stratification, as well as ISM and AMOC dynamics. Based on our paleo-PP record and modelling results, we can unravel the dynamical relationship between PP in the NE-BoB and the Indian Monsoon at both orbital- and millennial- timescales.

2. Site description and oceanographic setting

Core MD77-176 (14°30′5″N, 93°07′6″E) was retrieved from the northeastern BoB during the OSIRIS 3 cruise of the R.V. *Marion Dufresne* in 1977. The site lies ~200 km southwest of the modern Irrawaddy River mouth and is close to the limit between the northern BoB and the northern ADS. It is located on the continental slope at a water depth of 1375 m, which is above the modern lysocline of the BoB (Fig. 1a; Cullen and Prell, 1984). The lithology consists of olive grey terrigenous clay and silty clay layers with foraminifera- or nannofossil-bearing oozes (Colin et al., 2006).

The amplitude of seasonal changes in sea surface temperature (SST) in the BoB and the ADS is relatively small. The lowest (~26 °C) and highest SST (~28−29 °C) are recorded in winter and summer, respectively (Locarnini et al., 2010). The oceanic environment surrounding the studied site is under the influence of the Indian Monsoon and shows strong seasonal variations in evaporation/precipitation (Webster et al., 1998; Schott and McCreary, 2001; Shankar et al., 2002; Gadgil, 2003). During the summer, moisture-rich southwesterly winds blowing from the Indian Ocean result in heavy precipitation over South Asia, the BoB and the ADS (Fig. 1b, d; Lau et al., 2000; Chen et al., 2003; Randel and Park, 2006). During winter, dry and cool northeasterly surface winds, weaker than the summer winds, blow from Himalayan highlands to the ocean (Fig. 1c, e). The summer precipitation rates over the BoB and the ADS and over the surrounding lands (up to 15 mm/day) are much higher than that in the AS (Fig 1d, k). This heavy precipitation area covers the river catchments on the land surrounding the BoB and ADS, and thus generates massive freshwater discharge (up to 4050 km^3 a year) to the ocean (Sengupta et al., 2006). This input of freshwater generates a tongue of low sea surface salinity (SSS) occupying the northern BoB and ADS, whose extension is largest in November, several months later than the peak of summer precipitation (Akhil et al., 2014; Fournier et al., 2017; Fig. 1f, l). The low SSS tongue together with the direct rainfall on sea surface cause low SSS in the whole BoB and ADS (Duplessy et al., 1982; Akhil et al., 2014; Fig. 1f, g, l). Low SSS decreases sea surface density, thereby increasing the density gradient of the upper water column, and thus leading to a strong stratification that impedes the transfer of nutrient from the nutrient-rich deep layer into the euphotic zone. Such a "barrier layer" effect results in generally low annual PP in the BoB and ADS (Prasanna Kumar et al., 2002; Madhupratap et al., 2003; Fig. 1h, i). By contrast, evaporation is high with lower precipitation over the Arabian Sea, explaining that SSS than in the BoB (Fig. 1f, g, l), with subsurface flows of particularly high salinity waters originating from the Persian Gulf and the Red Sea. This high surface salinity and therefore the absence of a strong stratification make it possible the development of well-developed, wind-driven upwelling cells along the Somalian, Arabian and Indian coasts, which result in high PP in the AS (Anderson and Prell, 1992; Prasanna Kumar et al., 2001, 2009; McCreary et al., 2009). Although PP is generally low in the BoB and the ADS, seasonal variations can be seen at the studied site, with relatively higher PP during winter (Fig. 1m). This increased PP in winter is the result of increased SSS due to decreased precipitation, and increased mixing due to a secondary maximum in surface wind intensity (Fig. 1j, l). The low annual PP at the studied site indicates that this area is not significantly influenced by river input nutrients, which sustain extreme high PP in the near-shore and river mouth areas (Fig. 1h, i). Consequently, changes in the upper seawater column stratification and PP at the studied site are dominated by changes of SSS and wind-driven mixing.

3. Materials and Methods

3.1 Age model and sampling

The age model of core MD77-176 was established by Marzin et al., (2013) based on 31 Accelerator Mass Spectrometry ^{14}C ages measured on planktonic foraminifera *Globigerinoides ruber*. It was then refined by tuning the seawater oxygen isotope ($\delta^{18}O_{SW}$) anomaly curve with the GISP2 Greenland ice core $\delta^{18}O$ curve (Fig. 2). For the present study, we sampled the upper 711 cm of core MD77-176, every 3 cm. A total of 212 samples were analyzed, covering an interval ranging between 26 and 1 kyr BP, with temporal resolution varying from ~50 to 400 years.

3.2 Coccolith analysis and PP reconstruction

Slides for coccolith analysis were prepared using a "settling" technique described in Duchamp-Alphonse et al., (2018) after Beaufort et al., (2014). About 0.004 g of dry sediment was diluted in 28 mL Luchon™ water (pH = 8, bicarbonate = 78.1 mg/L, total dissolved solid = 83 mg/L) within a flat beaker and settled on a 12 × 12 mm coverslip for 4 h. After pumping the clear liquid out, the coverslip was then dried at 60°C in an oven, and mounted on slide with NOA74 glue. This technique ensures a homogenous distribution of coccoliths on the coverslip.
Slices were analyzed with a polarized light microscope (Leica DM6000B) at ×1000 magnification. For each slice, at least 500 coccolith specimens were counted by human eyes under at least 3 random fields of view. The relative abundance of *F. profunda* (Fp%) were calculated as: Fp% = 100 × (Fp number / total coccolith number). The 95% confidence interval for Fp% was calculated following the method of Patterson and Fishbein (1984), and corresponds to a reproducibility smaller than ±5 %.
Fp% indicates relative depth of nutricline which is critical for PP (Molfino and McIntyre, 1990a, 1990b). According to early studies, *F. profunda* thrives in the tropics and dwells at water depth of ~100–200 m, in the lower photic zone (Okada and Honjo, 1973). When nutricline gets shallower, more nutrient is brought into the upper euphotic zone leading to production increase of the upper euphotic zone coccolithophores, and thus lowering the relative abundance of the deep dwelling *F. profunda*. By contrast, when nutricline becomes deeper, the relative abundance of *F. profunda* increases. This relationship between Fp% and nutricline depth is the base for PP reconstructions via Fp% in marine sediment. Beaufort et al., (1997) first established a Fp%-PP empirical relationship in the AS based on the study of surface sediments. In this study, we estimated PP for the last 26 kyr using a recently published

https://doi.org/10.5194/cp-2020-27
Preprint. Discussion started: 6 March 2020

Fp%-PP empirical equation suited for tropical Indian Ocean (Hernández-Almeida et al., 2019): PP = [10^ (3.27 - 0.01 × Fp%)] × 365 / 1000. The unit of estimated PP is gram carbon per meter square per year (gC m^{-2} yr^{-1}).

3.3 Paleoclimate simulations

3.3.1 TraCE-21 simulation

TraCE-21 is a transient simulation of the global climate evolution over the last 22 kyr run with the CCSM3 model, designed by the National Center of Atmosphere Research (He et al., 2008; Collins et al., 2006a; Liu et al., 2009). CCSM3 is a global, coupled ocean-atmosphere-sea ice-land surface climate model, run without flux adjustment (Collins et al., 2006a). It includes four component models: the Community Atmospheric Model version 3 at T31 resolution (CAM3; Collins et al., 2006b), the Community Land Surface Model version 3 (CLM3; Dickinson et al., 2006), the Community Sea Ice Model version 5 (CSIM5; Briegleb et al., 2004), and the Parallel Ocean Program version 1.4.3 (POP; Smith and Gent, 2002). The forcing of the TraCE-21 simulation comprises changes in insolation due to the slow variations of astronomical parameters (ORB), changes in atmospheric greenhouse gases as measured in ice cores (GHG), modification of topography, land surface type and coastlines resulting from the evolution of the continental ice sheets as reconstructed by Peltier (2004) (ICE-5G), and changes in freshwater discharge from melting ice sheets which force the AMOC strength to change (MWF; Fig. 3a). In addition to the full TraCE-21 simulation (termed "TraCE" in the following), there are four single-forcing-sensitivity experiments: the ORB, GHG, MWF, and ICE, in which only one of the forcing mentioned above is allowed to evolve through time while all the three others are kept fixed at their 19 kyr BP value. More details about the TraCE can be found in He (2008). The datasets of TraCE and other experiments were downloaded from the website of Earth System Grid: https:// earthsystemgrid.org/project/trace.html. Atmosphere decadal-mean seasonal averaged and ocean decadal-mean annual averaged datasets were used in this study.

3.3.2 Experiments run with IPSL-CM5A-LR

IPSL-CM5A-LR (termed "CM5A" in the following) is an Earth System Model (ESM) developed at the "Institut Pierre Simon Laplace" (Dufresne et al., 2013) for the Coupled Model Intercomparison Project phase 5 (CMIP5; Taylor et al., 2012) and the Paleoclimate Modelling Intercomparison Project phase 3 (PMIP3; Braconnot et al., 2012) exercises. It is composed of the LMDZ5A atmospheric general circulation model (Hourdin et al., 2013), the ORCHIDEE land-surface model (Krinner et al., 2005) and the NEMO v3.2 ocean model (Madec, 2008) which includes the OPA9 ocean general circulation model, the LIM-2 sea-ice model, and the PISCES biogeochemical model (Aumount and Bopp, 2006). The atmospheric grid of this ESM model is regular in the horizontal with 96×95

https://doi.org/10.5194/cp-2020-27
Preprint. Discussion started: 6 March 2020

points in longitude × latitude (corresponding to a resolution of ~3.75°×1.9°) and 39 irregularly spaced vertical levels. The oceanic grid is curvilinear with 182×149 points, corresponding to a nominal resolution of 2°, and 31 vertical levels. It is refined close to the equator, where the resolution reaches ~0.5°.

Four experiments, set under different boundary conditions, were exploited in this study. Three of them were run for the PMIP3 exercise: the pre-industrial experiment (CTRL), the mid-Holocene experiment (MH), and the Last Glacial Maximum experiment (LGMc). Boundary conditions and more details for these three experiments can be found in Le Mézo et al. (2017). The fourth experiment (LGMf) is a freshwater "hosing" simulation (as in Kageyama et al., 2013), which was applied under LGM conditions. Compared to the LGMc experiment, the only difference is that an additional freshwater flux of 0.2 Sv was added over the North Atlantic and Nordic Seas and Arctic Ocean in the LGMf experiment. The freshwater flux causes the AMOC to slow down (Fig. 3b). The monthly outputs averaged over the last 100 years of each experiment were used in this study. Moreover, we used monthly results averaged over successive periods of 10 years for the LGMc and LGMf experiments to analyze the transient effects of the changes of AMOC strength.

4. Results and discussion

4.1 Paleoproductivity record in the northeastern Bay of Bengal

At the studied site, the main coccolith species are *Florisphaera profunda*, *Gephyrocapsa oceanica*, small *Gephyrocapsa* (*Gephyrocapsa* spp. <3µm) and *Emiliania huxleyi. F. profunda* varies between 60 % and 95 % and thus, largely dominates the assemblage over the last 26 kyr (Fig. 2 and S1). The high abundance of *F. profunda* in the studied core can be explained by the low surface nutrient concentration caused by strong stratification (section 2). Our results are coherent with high abundances of *F. profunda* observed in sediment trap records from the northern BoB (Stoll et al., 2007).

PP varies between 80 and 160 gC m^{-2} yr^{-1} (Fig. 2). Remarkably, estimated PP values (~125 gC m^{-2} yr^{-1}) of the late Holocene are very close to the modern annual PP mean (~135 gC m^{-2} yr^{-1}) of the studied area (Fig. S2). At orbital-scale, PP variations appear to be anti-phased with the northern hemisphere August insolation. Relatively high PP (~120 gC m^{-2} yr^{-1}) during the Last Glacial Maximum (LGM; 21–19 kyr BP) and the late Holocene (LH; 2 kyr BP to present) match low insolation periods. Conversely, relatively low PP (~100 gC m^{-2} yr^{-1}) during the early-middle Holocene (E-MH; 9–6 kyr BP) matches a high insolation period (Fig. 4a, h). Across the Holocene (11 kyr BP to present), PP first decreases, reaching a minimum between 8 and 6 kyr BP, and then increases upward, therefore showing an opposite trend compared to insolation (Fig. 4a, h). At millennial-scale, large magnitude PP oscillations, are observed during the deglaciation (19–11 kyr BP), showing similar features than those found in the Greenland ice core $\delta^{18}O$ record, representing the rapid climatic changes in north hemispheric high-latitude areas (Fig. 2; Stuiver and Grootes, 2000). High PP up to ~150 gC m^{-2} yr^{-1} and ~120 gC m^{-2} yr^{-1}, are found in the cold periods Heinrich stadial 1 (HS1, 17.0–14.8 kyr BP) and Younger Dryas (YD, 12.9–11.7 kyr BP) respectively. Low PP down to ~100 gC m^{-2} yr^{-1}, is found in the Bølling-Allerød warm period (B-A, 14.8–12.9 kyr BP) (Fig. 4h). In the time interval before the LGM (from 26 to 19 kyr BP), PP peaks with values higher than 140 gC m^{-2} yr^{-1} are observed at ~25, 23 and 21 kyr BP showing a ~2 kyr cycle in this interval (Fig. 4h).

The PP record of core MD77-176 is negatively correlated with the seawater oxygen isotope ($\delta^{18}O_{SW}$) anomaly obtained on the same core before the LGM, while a positive correlation can be seen between these two records during the deglaciation and the Holocene (19–1 kyr BP) (Fig. 4g, h). Since this $\delta^{18}O_{SW}$ record is interpreted as reflecting changes in salinity conditions in surface waters overlying site MD77-176 (Marzin et al., 2013), it appears that PP peaks are related to low SSS intervals before the LGM, and high SSS intervals over the last 19 kyr. The latter relationship is particularly obvious during HS1 and BA. From 19 to 14.8 kyr BP, the dramatic increase in PP (~70 gC m^{-2} yr^{-1} in amplitude) is associated with a ~6 psu increase of SSS (estimated using the modern $\delta^{18}O_{sw}$/salinity relationship that exists in the Northern Indian Ocean; Singh et al., 2010; Sijinkumar et al., 2016). On the contrary, the sharp decrease in PP (~40 gC m^{-2} yr^{-1} in amplitude) after 14.8 kyr BP, is accompanied by a significant drop in SSS (~5 psu in amplitude).

4.2 Influence of North Atlantic climate and Indian Summer Monsoon on PP

4.2.1 Last glacial: 26 to 19 kyr BP

Several pieces of evidence suggest that millennial-scale variations of PP between 26 and 19 kyr (i.e. before the LGM) chiefly resulted from wind-driven mixing. First, high PP values are reached during intervals of low surface water salinity. If these PP variations (and upper water column stratification) were primarily driven by precipitation – evaporation changes, the opposite relationship would be expected, and PP would peak at periods of higher salinity because of the weaker barrier layer effect. Besides, according to the record of $\delta^{18}O_{SW}$ difference between surface and subsurface seawaters obtained in the ADS, which is used as an upper water vertical stratification proxy, it appears that no significant variations occurred in upper ocean salinity stratification before the LGM (Gebregiorgis et al., 2016). Second, the speleothem $\delta^{18}O$ signal in North India (Fig. 4c; Dutt et al., 2015), the $\delta D_{alkanes}$ record in the N-BoB (Fig. 4d; Contreras-Rosales et al., 2014), as well as the Ba/Ca$_{G.\ sacculifer}$ record in the Andaman Sea (Fig. 4f, Gebregiorgis et al., 2016) all document a long-lasting dry phase and heavily reduced river runoff in the area before the LGM, implying a subdued influence of freshwater inputs within the BoB and the ADS, either directly (decreased precipitation over the sea) or from reduced river runoff. Third, the relationship between PP and SSS is

https://doi.org/10.5194/cp-2020-27
Preprint. Discussion started: 6 March 2020

similar to that observed in western and northern Arabian Sea, where PP pattern is primarily controlled by surface wind strength (Fig. 4i–k; Ivanochko et al., 2005; Schulz et al. 1998; Anand et al., 2008). Indeed, over the last 26 kyr, enrichments of organic carbon and Ba in sediments appear to reflect strong-southwesterly wind-induced biological productivity, when $\delta^{18}O$ values document low SSS conditions (Fig.4i–k). At last, this is in line with overall ISM reconstructions documenting cool and dry conditions in the northern Indian Ocean during the strong glaciation period (Cullens, 1981; Duplessy, 1982; Kudrass et al., 2001; Contreras-Rosales et al., 2014; Dutt et al., 2015) due to enhanced snow accumulation and relatively low temperatures in the Tibetan Plateau and Himalaya (Shi Y, 2002; Mark et al., 2005) that cause a weakened meridional thermal land-sea gradient and an equatorward shift of the ITCZ mean position (Kudrass et al., 2001; Overpeck et al., 1996; Sirocko et al., 1996; Cai et al., 2012).

4.2.2 Last deglaciation to present (19 – 1 kyr BP)

The factors controlling PP on the millennial-scale over the last 19 kyr, appear to differ from those acting before the LGM. A strong impact of wind-related changes on vertical stratification is unlikely given that river runoff (Gebregiorgis et al., 2016), together with the precipitation (Dutt et al., 2015; Contreras-Rosales et al., 2014), gradually strengthened in this area during the last deglaciation up to the mid-Holocene, due to stronger southwest monsoon circulation (Fig. 4c–g). Since site MD77-176 is directly influenced by river discharges and because PP positively covaries with SSS during that time interval (Fig. 4g, h), it seems reasonable to propose that those PP variations are driven by ISM dynamic through changes in upper water column stratification associated to SSS variations (Govil and Naidu, 2011). In such a scenario, we suggest that the gradual increases of PP during HS1 and YD reflect the shoaling of the nutricline in response to increased salinity of the mixed layer resulting from a weaker summer (wet) southwest monsoon and strongly reduced river runoff (Sinha et al., 2005; Govil and Naidu, 2011; Dutt et al., 2015; Contreras-Rosales et al., 2014, Phillips et al., 2014; Gebregiorgis et al., 2016). On the contrary, PP minima observed during the B-A and the early to mid-Holocene testify for a stronger stratification and a deeper nutricline, due to stronger South Asian Monsoon precipitation (Sinha et al., 2005).

Some influence from the North Atlantic climate is also likely, given that, during the last deglaciation, events of high (low) PP and SSS in the BoB (Rashid et al., 2007; Marzin et al., 2013), i.e. weak (strong) ISM, correspond to cold HS1 and YD (warm B-A) events in the North Atlantic, as defined by the GISP2 Greenland ice core $\delta^{18}O$ record on Fig. 2. The abrupt changes in the North Atlantic climate have been widely associated with changes in the AMOC (Elliot et al., 2002; McManus et al., 2004; Stocker and Johnsen, 2003). A widely held explanation for these rapid climatic changes involves the supply of fresh water to the northern Atlantic Ocean and its direct effect on the transport of heat to mid and low latitudes, via a decrease and even a collapse, of the AMOC (Heinrich, 1988). In such a scenario, the AMOC is usually seen as a conveyor belt involved in interhemispheric transport of heat (e.g.

https://doi.org/10.5194/cp-2020-27
Preprint. Discussion started: 6 March 2020

Liu et al., 2009; Buckley and Marshall, 2016), whose changes have a specific influence on tropical Atlantic rainfall (Wang et al., 2004; Peterson et al., 2000; Peterson and Haug, 2006; Swingedouw et al., 2009), and ISM (Overpeck et al., 1996; Barber et al., 1999; Fleitmann et al., 2003; Gupta et al., 2003; Murton et al., 2010; Yu et al., 2010; Cai et al., 2012; Marzin et al., 2013). Therefore, it is not excluded that our PP record is sensitive to such processes. However, as anti-phase relationships between our PP record and those in the N- and W-AS are observed, it implies that the mechanism involving the influence of AMOC on PP in the northeastern BoB, is different from that in the AS related to wind-induced upwelling and mixing (Schultz et al., 1998; Altabet et al., 2002; Ivanochko et al., 2005). One plausible explanation is that during HS1 and YD, releases of meltwaters in the northern Atlantic Ocean subdued or disrupted the AMOC, thus triggering a southward shift of the ITCZ, a large decrease in Indian Monsoon precipitation (Gupta et al., 2003; Goswami et al., 2006; Li et al., 2008; Pausata et al., 2011), and leading to an increased PP in the BoB due to saltier surface sea waters. However, even if our record supports the scenario of a major role of the AMOC in rapid deglacial PP changes, there are still major unresolved issues regarding the mechanisms at play. In particular, the evidence linking PP changes with upper water column stratification in the context of past ISM and AMOC variabilities is still incomplete.

4.3 PP dynamics over the last 19 kyr: data-model combined arguments

As mentioned above, PP variations in the northeastern BoB over the last 19 kyr have a close linkage to local SSS changes related to Indian Monsoon precipitation. In order to better understand the mechanisms behind PP response, we analyzed climate model outputs (section 3.3). We focused on the Holocene and the deglaciation to investigate the effect of insolation and AMOC strength on the Indian Monsoon and try and understand how the Indian Monsoon influences PP in the northeastern BoB during a period of AMOC change.

4.3.1 Impacts of insolation and AMOC on the Indian Summer Monsoon and local hydrological conditions

During the Holocene, insolation is the main climate forcing factor since other forcing (i.e. greenhouse gas, ice volume, coastlines, vegetation) are relatively stable after the deglaciation. The mechanisms that force monsoon climate to change were studied by many modeling works (Kutzbach, 1981; Kutzbach and Street-Perrott, 1985; Braconnot et al., 2007a, 2007b; Marzin and Braconnot, 2009; Zhao and Harrison, 2012; Kageyama et al., 2013). During the last deglaciation, the AMOC strength showed large fluctuations (McManus et al., 2004) and modeling studies focused on the impact of AMOC variations on the Asian Monsoon (e.g. Zhang and Delworth, 2005; Lu et al., 2006; Marzin et al., 2013; Liu et al., 2014; Wen et

https://doi.org/10.5194/cp-2020-27
Preprint. Discussion started: 6 March 2020

al., 2016). Regarding precipitation changes over South Asia, Marzin et al. (2013) proposed that AMOC can remotely impact the Indian monsoon via perturbations of the subtropical jet over Africa and Eurasia triggered by atmospheric and oceanic changes over the tropical Atlantic.

Here, to illustrate the general impacts of insolation on the Indian Monsoon and local hydrological changes, we studied the differences of summer wind vectors, annual mean precipitation and annual mean SSS between the MH and the CTRL experiment run with CM5A (Fig. S3c, d), and between the MH (6.5−5.5 kyr BP mean) and LH (1.5−0.5 kyr BP mean) in the TraCE and ORB experiments (section 3.3; Fig. S4). To test the impact of AMOC variation, we studied the differences of the same parameters between the LGMc and LGMf (Figs. 3a and S3a, b), between the LGM (21−19 kyr BP mean) and HS1 (17−15.5 kyr BP mean), and between the B-A (14.8−14 kyr BP mean) and HS1 in the TraCE and MWF experiments (section 3.3; Figs. 3a, S5 and S6). The results of CM5A show increased South Asia precipitation and decreased SSS in BoB and ADS in the MH compared to the CTRL, while such trends are less obvious in the TraCE and ORB experiments (Fig. S4). The experiments involving changes of AMOC conditions depict similar results. They both show that enhanced (weakened) AMOC conditions observed during the LGM and the B-A (HS1) are associated with decreased (increased) SSS and increased (decreased) stratification in the studied area (Fig. 5), while no striking trends may be highlighted for SST during these time intervals.

In the TraCE simulation, we first investigated the changes in annual mean seawater salinity at 5m (SSS), seawater temperature at 5m (SST), and upper seawater stratification in the northeastern BoB over the last 19 kyr (Fig. 5 and S7). The density difference between the surface (5 m) and 200 m is a useful measure of stratification (ΔPD_200-5; Behrenfeld et al., 2006). Such numerical results clearly support our PP results and previous interpretations and is in good accordance with the modern "barrier effect" associated to low SSS conditions. Similarly, a good correlation exists between the simulated SSS changes and the SSS record of MD77-176 during the deglaciation. The oscillations of simulated ΔPD_200-5 and SSS in the deglaciation are chiefly accounted for by the MWF forcing as shown by the outputs of the MWF sensitivity experiment (Fig. S8). However, during the Holocene, the simulated ΔPD_200-5 and SSS in the TraCE simulation fail to reproduce the successive decreasing and then increasing trends observed in PP and SSS records from core MD77-176 (Fig. 5), which we have attributed to orbital forcing. The outputs of the ORB sensitivity experiment show limited and even opposite trends to what we observed (Fig. S8). As mentioned above, the results of IPSL show large differences of SSS between the MH and the pre-industrial period, which is identical to what the sedimentary reconstruction of SSS shows (Sijinkumar et al., 2016). This indicates that the CM5A has probably a higher sensitivity to the orbital

https://doi.org/10.5194/cp-2020-27
Preprint. Discussion started: 6 March 2020

insolation forcing than the CCSM3. Moreover, the difference of precipitation between MH and CTRL experiments in the eastern BoB (ADS) is negative, which is opposite to the difference occurring in the South Asia (Fig. S3c). However, the SSS decreased in the whole BoB (ADS) during the MH compared to the CTRL, which means that river runoff is a much larger contributor of freshwater input than direct rainfall on the sea, and is thus the main driver of SSS changes in the BoB and ADS (Behara and Vinayachandran, 2016).

4.3.2 PP response to hydrological changes

The largest PP variations occur during the deglaciation. The outputs of MWF experiment also show strong responses of SSS and ΔPD_200-5 to the changes of AMOC strength forced by meltwater discharge in the North Atlantic (Fig. S8). Therefore, we analyzed how PP in the northeastern BoB responds to AMOC changes in the ESM including the marine biogeochemical component PISCES.

We analyzed the LGMc and LGMf experiments (section 3.3.2), and the results shown here are the mean of winter months, from December to February (DJF) in the northern BoB (Fig. S7 shows the grids from which the results have been extracted). In the LGMf, the AMOC is progressively getting weaker during the duration of the run (Fig. 3b). Under weakening AMOC conditions, SSS in the northern BoB is getting higher (Fig. 6d). Similar to the results of TraCE, the change of SSS contributes to the change of stratification in CM5A (Fig. 6d). The smaller ΔPD_200-5 (weaker stratification) causes the integrated nitrate content of the upper 50 m (NO3_0-50 for short) to increase, and a negative correlation can be seen between them (Fig. 6b). The increasing upper nitrate content results in an increase of the integrated PP, and a positive correlation can be seen between them (Fig. 6a). Consequently, the increased PP is related to weakened stratification caused by higher SSS (Fig. 6c).

Vertical profiles of the four parameters discussed above (namely: salinity, density, NO3 and PP) were also investigated (Figs. 7 and 8). They show the contrasted response of nitrate concentration in the upper water column (above 40 m) and the lower water column (below 60 m) associated to AMOC reduction. While the upper-water nitrate content increases, the lower-water nitrate content decreases, and the increase is much lower than the decrease (Fig. 8a). Conversely, the PP increase in the upper layer is larger than the decrease in the subsurface (Fig. 8b). This is because photosynthesis rate is much higher in the upper euphotic layer than in the lower euphotic layer, but the upper seawater is nutrient limited. Therefore, PP variations in the NE-BoB driven by changes of AMOC intensity are linked to the upper nutrient availability, which is controlled by the salinity-related stratification.

The results discussed above are for the DJF mean because modern data show that the highest PP takes place in winter, which contributes about half of the annual gross PP (Fig. 1m). We propose that this mechanism revealed

https://doi.org/10.5194/cp-2020-27
Preprint. Discussion started: 6 March 2020

Climate of the Past
Discussions

by the DJF mean results of the experiments run with CM5A involving the changed AMOC explains the PP changes in the deglaciation given by our PP record reconstructed by coccoliths assemblages.

5. Conclusion

We have reconstructed a PP record for the northeastern BoB over the last 26 kyr, using an empirical equation relating Fp% to PP. From 26 to19 kyr BP (including the LGM), data suggest that PP in the northeastern BoB was probably controlled by upper water wind mixing, while relatively dry climate conditions and reduced freshwater inputs to the ocean, prevailed. Over the last 19 kyr, the PP variations in the NE-BoB are anti-phased with those previously reconstructed for the western and northern AS, and with SSS reconstructions obtained on the same core. Such relationships point that, as for modern setting, the BoB received generally heavier annual precipitations than the AS, and that salinity-related-stratification controlled PP. Stratification changes are driven by Indian Monsoon precipitation dynamic, that generates variations in freshwater supplies to the ocean. The analysis of climate model outputs provides additional evidences for that salinity-stratification mechanism. Together with our PP record and published paleo-climatological and paleo-hydrological records, it demonstrates that during the deglaciation, salinity stratification is related to monsoon precipitation dynamics, which is chiefly forced by insolation and the strength of AMOC. The dramatic decrease of PP in the B-A compare to the HS1 is mainly due to the recovered AMOC which strengthen ISM and upper seawater stratification.

Data avalibility

Data to this paper can be required. Please contact the X. Zhou or S. Duchamp-Alphonse.

Supplement

The supplement related to this article is available online

Author contribution

XZ, SDA, MK and CC developed the idea. CC and FB provided sediment samples. XZ did coccolith analysis and visualization of the climate modelling results. The datasets of climate model IPSL-CM5A-LR were provided by MK. FB and LB joined the discussion and gave additional ideas for the manuscript. All authors contribute to the manuscript writing.

Competing interests

The authors declare that they have no conflict of interest.

Acknowledgements

X. Zhou was supported by a PhD scholarship from the China Scholarship Council (CSC) and thank Laboratoire des Sciences du Climat et de l'Environnement (LSCE) for admitting his study related to climate model. The work in this manuscript was supported by the French Centre national de la recherche scientifique (CNRS).

Reference

Akhil, V. P., Durand, F., Lengaigne, M., Vialard, J., Keerthi, M. G., Gopalakrishna, V. V., Deltel, C., Papa, F. and de Boyer Montegut, C.: A modeling study of the processes of surface salinity seasonal cycle in the Bay of Bengal., Journal of Geophysical Research: Oceans, 119, 3926–3947, 2014.

Altabet, M. A., Higginson, M. J. and Murray, D. W.: The effect of millennial-scale changes in Arabian Sea denitrification on atmospheric CO_2, Nature, 415, 159–162, 2002.

Anand, P., Kroon, D., Singh, A. D., Ganeshram, R. S., Ganssen, G and Elderfield, H.: Coupled sea surface temperature–seawater $\delta^{18}O$ reconstructions in the Arabian Sea at the millennial scale for the last 35 ka, Paleoceanography, 23, PA4207, 2008.

Anderson, D. M. and Prell, W. L.: The structure of the southwest monsoon winds over the Arabian Sea during the late Quaternary: observation, simulations, and marine geologic evidence, Journal of Geophysical Research, 97, 15481–15487, 1992.

Aumont, O. and Bopp, L.: Globalizing results from ocean in situ iron fertilization studies, Global Biogeochemical Cycle, 20, GB2017, 2006.

Barber, D. C., Dyke, A., Hillaire-Marcel, C., Jennings, A. E., Andrews, J. T., Kerwin, M. W., Bilodeau, G., McNeely, R., Southon, J., Morehead, M. D. and Gagnon, J.-M.: Forcing of the cold event of 8,200 years ago by catastrophic drainage of Laurentide lakes, Nature, 400, 344–348, 1999.

Beaufort, L., Lancelot, Y., Camberlin, P., Cayre, O., Vincent, E., Bassinot, F. and Labeyrie, L.: Insolation cycles as a major control of Equatorial Indian Ocean primary production, Science, 278, 1451–1454, 1997.

Beaufort, L., Barbarin, N. and Gally, Y.: Optical measurements to determine the thickness of calcite crystals and the mass of thin carbon particles such as coccoliths, Nature Protocols, 9, 633–642, 2014.

Behara, A. and Vinayachandran, P. N.: An OGCM study of the impact of rain and river water forcing on the Bay of Bengal, Journal of Geophysical Research: Oceans, 121, 2425–2446, 2016.

https://doi.org/10.5194/cp-2020-27
Preprint. Discussion started: 6 March 2020

Behrenfeld, M. J., O'Malley, R. T., Siegel, D. A., McClain, C. R., Sarmiento, J. L., Feldman, G. C., Milligan, A. J., Falkowski, P. G., Letelier, R. M. and Boss, E. S.: Climate-driven trends in contemporary ocean productivity, Nature, 444, 752–755, 2006.

Braconnot, P., Otto-Bliesner, B., Harrison, S., Joussaume, S., Peterchmitt, J.-Y., Abe-Ouchi, A., Crucifix, M., Driesschaert, E., Fichefet, Th., Hewitt, C. D., Kageyama, M., Kitoh, A., Laîné, A., Loutre, M.-F., Marti, O., Merkel, U., Ramstein, G., Valdes, P., Weber, S. L., Yu, Y., and Zhao, Y.: Results of PMIP2 coupled simulations of the Mid-Holocene and Last Glacial Maximum – Part 1: experiments and large-scale features, Climate of the Past, 3, 261–277, 2007a.

Braconnot, P., Otto-Bliesner, B., Harrison, S., Joussaume, S., Peterchmitt, J.-Y., Abe-Ouchi, A., Crucifix, M., Driesschaert, E., Fichefet, Th., Hewitt, C. D., Kageyama, M., Kitoh, A., Loutre, M.-F., Marti, O., Merkel, U., Ramstein, G., Valdes, P., Weber, L., Yu, Y., and Zhao, Y.: Results of PMIP2 coupled simulations of the Mid-Holocene and Last Glacial Maximum – Part 2: feedbacks with emphasis on the location of the ITCZ and mid- and high latitudes heat budget, Clim. Past, 3, 279–296, https://doi.org/10.5194/cp-3-279-2007, 2007b.

Braconnot, P., Harrison, S. P., Kageyama, M., Bartlein, P. J., Masson-Delmotte, V., Abe-Ouchi, A., Otto-Bliesner, B., and Zhao, Y.: Evaluation of climate models using palaeoclimatic data, Nature Climate Change, 2, 417–424, 2012.

Briegleb, B. P., Bitz, C. M., Hunke, E. C., Lipscomb, W. H., Holland, M., Schramm, J. L. and Moritz, R. E.: Scientific description of the sea ice component in the Community Climate System Model, Version 3, University Corporation for Atmospheric Research, 2004.

Buckley, M. W. and Marshall, J.: Observations, inferences, and mechanisms of the Atlantic Meridional Overturning Circulation: A review, Reviews of Geophysics, 54, 5–63, 2016.

Cai, Y., Zhang, H., Cheng, H., An, Z., Edwards, R. L., Wang, X., Tan, L., Liang, F., Wang, J. and Kelly, M.: The Holocene Indian Monsoon variablility over the southern Tibetan Plateau and its teleconnections, Earth and Planetary Science Letter, 335–336, 135–144, 2012.

Chen, T.-C.: Maintenance of summer monsoon circulations: a planetary-scale perspective, Journal of Climate, 16, 2022–2037, 2003.

Chiba, S., Ono, T., Tadokoro, K. and Midorikawa, T.: Increased stratification and decreased lower trophic level productivity in the Oyashio Region of the North Pacific: A 30-year retrospective study, Journal of Oceanography, 60, 149–162, 2004.

Clark, P. U., Shakun, J. D., Baker, P. A.: Global climate evolution during the last deglaciation: PNAS, 109, E1134–E1142, 2012.

Clement, A. C. and Peterson, L. C.: Mechanisms of abrupt climate change of the last glacial period, Reviews of Geophysics, 46, RG4002, 2008.

Colin, C., Turpin, L., Blamart, D., Frank, N., Kissel, C. and Duchamp, S.: Evolution of weathering patterns in the Indo-Burman Ranges over the last 280 kyrs: Effect of sediment provenance on 87Sr/86Sr ratios tracer, Geochemistry, Geophysics, Geosystems, 7, Q03007. 2006.

Collins, W. D., Bitz, C. M., Blackmon, M. L., Bonan, G. B., Bretheton, C. S., Carton, J. A., Chang, P., Doney, S. C., Hack, J. J., Henderson, T. B., Kiehl, J. T., Large, W. G., McKenna, D. S., Santer, B. D. and Smith, R. D.: The Community Climate System Model Version 3 (CCSM3), Journal of Climate, 19, 2122–2143, 2006a.

Collins, W. D., Rasch, P. J., Boville, B. A., Hack, J. J., McCaa, J. R., Williamson, D. L. and Briegleb, B. P.: The formulation and atmospheric simulation of the Community Atmosphere Model Version 3 (CAM3), Journal of Climate, 19, 2144–2161, 2006b.

Contreras-Rosales, Jennerjahn, T., Tharammal, T., Meyer, V., L. A., Lückge, A., Paul, A. and Schefuß, E.: Evolution of the Indian Summer Monsoon and terrestrial vegetation in the Bay of Bengal region during the past 18 ka, Quaternary Science Reviews, 102, 133–148, 2014.

Cullen, J. L.: Microfossil evidence for changes salinity patterns in the Bay of Bengal over the last 20 000 years, Palaeogeography, Palaeoclimatology, Palaeoecology, 35, 315–356, 1981.

Cullen, J. L and Prell, W. L.: Planktonic foraminifera of the northern Indian Ocean: Distribution and preservation in surface sediments, Marine Micropaleontology, 9, 1–52, 1984.

Currie, J. C., Lengaigne, M., Vialard, J., Kaplan, D. M., Aumont, O., Naqvi, S. W. A. and Maury, O.: Indian Ocean Dipole and El Niño/Southern Oscillation impacts on regional chlorophyll anomalies in the Indian Ocean, Biogeosciences, 10, 6677–6698, 2013.

Dey, S., Singh, R. P.: Comparison of chlorophyll distribution in the northeastern Arabian Sea and southern Bay of Bengal using IRS-P4 Ocean Color Monitor data, Remote Sensing of Environment, 85, 424–428, 2003.

Dickinson, R. E., Oleson, K. W., Bonan, G., Hoffman, F., Thirnton, P., Vertenstein, M., Yang, Z.-L. and Zeng, X.: The Community Land Model and its climate statistics as a component of the Community Climate System Model, Journal of Climate, 19, 2302–2324, 2006.

Duchamp-Alphonse, S., Siani, G, Michel, E., Beaufort, L, Gally, Y. and Jaccard, S. L.: Enhanced ocean-atmosphere carbon partitioning via the carbonate counter pump during the last deglacial, Nature Communications, 9, 2396, 2018.

Dutt, S., Gupta, A. K., Clemens, S. C., Cheng, H., Singh, R. K., Kathayat, G and Edwards, R. L.: Abrupt changes in Indian summer monsoon strength during 33,800 to 5500 years B.P., Geophysical Research Letters, 42, 5526–5532, 2015.

https://doi.org/10.5194/cp-2020-27
Preprint. Discussion started: 6 March 2020

Climate of the Past Discussions

Dufresne, J.-L., Foujols, M.-A., Denvil, S., et al: Climate change projections us- ing the IPSL-CM5 Earth System Model: from CMIP3 to CMIP5, Climate Dynamics, 40, 2123–2165, 2013.

Duplessy, J. C.: Glacial to interglacial contrasts in the northern Indian Ocean, Nature, 195, 494–498, 1982.

Elliot, M., Labeyrie, L. and Duplessy, J.-C.: Changes in North Atlantic deep-water formation associated with the Dansgaard-Oeschger temperature oscillations (60–10 ka), Quaternary Science Reviews, 21, 1153–1165, 2002.

Fleitmann, D., Burns, S. J., Mudelsee, M., Neff, U., Kramers, J., Mangini, A. and Matter, A.: Holocene forcing of the Indian Monsoon recored in a stalagmite from southern Oman, Science, 300, 1737–1739, 2003.

Fournier, S., Vialard, F., Lengaigne, M., Lee, T., Gierach, M. M. and Chaitanya, A. V. S.: Modulation of the Ganges-Brahmaputra River Plume by the Indian Ocean Dipole and Eddies inferred from satellite observations, Journal of Geophysical Research: Ocean, 122, 9591–9604, 2017.

Gadgil, S.: The Indian Monsoon and its variability, Annual Review of Earth Planetary Science, 31, 429–467, 2003.

Gauns, M., Madhupratap, M., Ramaiah, N., Jyothibabu, R., Fernandes, V., Paul, J. T. and Prasanna Kumar, S.: Comparative accounts of biological productivity characteristics and estimates of carbon fluxes in the Arabian Sea and the Bay of Bengal, Deep-Sea Research Ⅱ, 52, 2003–2017, 2005.

Gebregiorgis, D., Hathorne, E. C., Sijinkumar, A. V., Nagender Nath, B., Nürnberg, D.: South Asian summer monsoon variability during the last ~54 kyrs inferred from surface salinity and river runoff proxies, Quaternary Science Reviews, 138, 6–15, 2016.

Goswami, B. N., Madhusoodanan, M. S., Neema, C. P. and Sengupta, D.: A physical mechanism for North Atlantic SST influence on the Indian summer monsoon, Geophysical Research Letters, 33, L02706, 2006.

Govil, P. and Naidu, P. D.: Variations of Indian monsoon precipitation during the last 32 kyr reflected in the surface hydrography of the Western Bay of Bengal, Quaternary Science Reviews, 30, 3871–3879, 2011.

Gupta, A. K., Andrews, D. M. and Overpeck, J. T.: Abrupt changes in the Asian southwest monsoon during the Holocene and their links to the North Atlantic Ocean, Nature, 421, 354–357, 2003.

He, F.: Simulating transient climate evolution of the last deglaciation with CCSM3, PhD. dissertation, University of Wisconsin-Madison, 2008.

Heinrich, H.: Origin and consequences of cyclic ice rafting in the northeast Atlantic Ocean during the past 130,000 years, Quaternary Research, 29, 142–152, 1988.

Hernández-Almeida, I., Ausín, B., Saavedra-Pellitero, M., Baumann, K.-H. and Stoll, H. M.: Quantitative reconstruction of primary productivity in low latitudes during the last glacial maximum and the mid-to-late Holocene from a global *Florisphaera profunda* calibration dataset, Quaternary Science Reviews, 205, 166–181, 2019.

https://doi.org/10.5194/cp-2020-27
Preprint. Discussion started: 6 March 2020

Climate of the Past Discussions

Hourdin, F., Foujols, M.-A., Codron, F., Guemas, V., Dufresne, J.- L., Bony, S., Denvil, S., Guez, L., Lott, F., Ghattas, J., Braconnot, P., Marti, O., Meurdesoif, Y., and Bopp, L.: Impact of the LMDZ atmospheric grid configuration on the climate and sensitivity of the IPSL-CM5A coupled model, Clim. Dynam., 40, 2167–2192, https://doi.org/10.1007/s00382-012-1411-3, 2013.

Ivanochko, T. S., Ganeshram, R. S., Brummer, G. A., Ganssen, G., Jung, S. J. A., Moreton, S. G. and Kroon, D.: Variations in tropical convection as an amplifier of global climate change at the millennial scale, Earth and Planetary Science Letters, 235, 302–314, 2005.

Ivanova, E., Schiebel, R., Singh, A. D., Schmiedl, G., Niebler, H.-S. and Hemleben, C.: Primary production in the Arabian Sea during the last 135 000 years, 197, 61–82, 2003.

Kageyama, M., Merkel, U., Otto-Bliesner, B., Prange, M., Abe-Ouchi, A., Lohmann, G., Ohgaito, R., Roche, D. M., Singarayer, J., Swingedouw, D. and Zhang, X.: Climatic impacts of fresh water hosing under Last Glacial Maximum conditions: a multi-model study, Climate of the Past, 9, 935–953, 2013.

Keen, T. R., Kindle, J. C. and Young, D. K: The interaction of southwest monsoon upwelling, advection and primary production in the northwest Arabian Sea, Journal of Marine Systems, 61–82, 1997.

Krinner, G., Viovy, N., de Noblet-Ducoudré, N., Ogée, J., Polcher, J., Friedlingstein, P., Ciais, P., Sitch, S., and Prentice, I. C.: A dynamic global vegetation model for studies of the cou- pled atmosphere-biosphere system, Global Biogeochemistry Cycle, 19, GB1015, 2005.

Kudrass, H. R., Hofmann, A., Doose, H., Emeis, K. and Erlenkeuser, H.: Modulation and amplification of climatic changes in the Northern Hemisphere by the Indian summer monsoon during the past 80 k.y., Geology, 29, 63–66, 2001.

Kutzbach, J. E.: Monsoon Climate of the Early Holocene: Climate Experiment with the Earth's Orbital Parameters for 9000 Years Ago, Science, 214, 59–61, 1981.

Kutzbach, J. E. and Street-Perrott, F. A: Milankovitch forcing of fluctuations in the level of tropical lakes from 18 to 0 kyr BP, Nature, 317, 130–134, 1985.

Lau, K.-M., Kim, K.-M., Yang, S.: Dynamicsal and boundary forcing characteristics of regional components of the Asian Summer Monsoon, Journal of Climate, 13, 2461–2482, 2000.

Le Mézo, P., Beaufort, L., Bopp, L., Braconnot, P and Kageyama, M.: From monsoon to marine productivity in the Arabian Sea: insights from glacial and interglacial climates, Climate of the Past, 13, 759–778, 2017.

Lévy, M., Klein, P and Treguier, A.-M.: Impact of sub-mesoscale physics on production and subduction of phytoplankton in an oligotrophic regime, journal of Marine Research, 59, 535–565, 2001.

Li, S., Perlwitz, J., Quan, X. and Hoerling, M. P.: Modelling the influence of North Atlantic multidecadal warmth on the Indian summer rainfall, Geophysical Research Letters, 35, L05804, 2008.

https://doi.org/10.5194/cp-2020-27
Preprint. Discussion started: 6 March 2020

Li, J., Liu, S., Shi, X., Zhang, H., Fang, X., Cao, P., Yang, G., Xue, X., Khokiattiwong, S. and Kornkanitnan, N.: Sedimentary responses to the sea level and Indian summer monsoon changes in the central Bay of Bengal since 40 ka, Marine Geology, 415, 105947, 2019.

Liu, Z., Otto-Bliesner, B. L., He, F., Brady, W. C., Tomas, R., Clark, P. U., Carlson, A. E., Lynch-Stieglitz, J., Curry, W., Brook, E., Erickson, D., Jacob, R., Kutzbach, J. and Cheng, J.: Transient Simulation of Last Deglaciaiton with a new mechanism for Bølling-Allerød Warming, Science, 325, 310–314, 2009.

Liu, Z., Wen, X., Brady, E. C., Otto-Bliesner, B., Yu, G., Lu, H., Cheng, H., Wang, Y., Zheng, W., Ding, Y., Edwards, R. L., Cheng, J., Liu, W. and Yang, H.: Chinese cave records and the East Asia Summer Monsoon, Quaternary Science Reviews, 83, 115–128, 2014.

Locarnini, R. A., Mishonov, A. V., Antonov, J. I., Boyer, T. P., Garcia, H. E., Baranova, O. K., Zweng, M. M., Johnson, D. R.: World ocean atlas 2009, In: Levitus, S. (Ed.), Temperature, 1. Government Printing Office, Washington, D.C., p. 184. NOAA Atlas NESDIS 68, 2010.

Lu, R., Dong, B. and Ding, H.: Impact of the Atlantic Multidecadal Oscillation on the Asian summer monsoon, Geophysical Research Letters, 33, L24701, 2006.

Madhupratap, M., Gauns, M., Ramaiah, N., Prasanna Kumar, S., Muraleedharan, P. M., Sousa, S. N. and Muraleedharan, U.: Biogeochemistry of the Bay of Bengal: physical, chemical and primary productivity characteristics of the central and western Bay of Bengal during summer monsoon 2001, Deep-Sea Research Ⅱ, 50, 881–896, 2003.

Mark, B. G., Harrison, S. P., Spessa, A., New, M., Evans, D. J. A. and Helmens, K. F.: Tropical snowline changes at the last glacial maximum: A global assessment, Quaternary International, 138–139, 168–201, 2005.

Marzin, C. and Braconnot, P.: Variations of Indian and African monsoons induced by insolation changes a 6 and 9.5 kyr BP, Climate Dynamics, 33, 215–231, 2009.

Marzin, C., Kallel, N., Kageyama, M., Duplessy, J.-C. and Braconnot, P.: Glacial fluctuations of the Indian monsoon and their relationship with North Atlantic climate: new data and modeling experiments, Climate of the Past. 9, 2135–2151, 2013.

Madec, G.: NEMO ocean engine, Note du pôle de modélisation, Institut Pierre-Simon Laplace (IPSL), France, No. 27 ISSN No. 1288-1619, 2008.

Meehl, G. A.: Couple land-ocean-atmosphere processes and South Asian Monsoon variability, Science, 266, 263–267, 1994.

Meehl, G. A.: The South Asian Monsoon and the Tropospheric Biennial Oscillation, Journal of Climate, 10, 1921–1943, 1997.

https://doi.org/10.5194/cp-2020-27
Preprint. Discussion started: 6 March 2020

McCreary, J. P., Murtugudde, R., Vialard, J., Vinayachandran, P. N., Wiggert, J. D., Hood, R. R., Shankar, D. and Shetye, S.: Biophysical processes in the Indian Ocean, Geophysical Monograph Series, 2009.

McManus, J. F., Francois, R., Gherardi, J.-M., Keigwin, L. D. and Brown-Leger, S.: Collapse and rapid resumption of Atlantic meridional circulation linked to deglacial climate changes, Nature, 834–837, 2004.

Molfino, B. and McIntyre, A.: Precessional forcing of nutricline dynamics in the Equatorial Atlantic, Science, 249, 766–769, 1990a.

Molfino, B. and McIntyre, A.: Nutricline variation in the Equatorial Atlantic coincident with the Younger Dryas, Paleoceanography, 5, 997–1008, 1990b.

Murton, J. B., Bateman, M. D., Dallimore, S. R., Teller, J. T. and Yang, Z.: Identification of Younger Dryas outburst flood path from Lake Agassiz to the Arctic Ocean, Nature, 464, 740–743, 2010.

Okada, H. and Honjo, S.: The distribution of oceanic coccolithophorids in the Pacific, Deep-Sea Research, 20, 355–374, 1973.

Overpeck, J., Anderson, D., Trumbore, S. and Prell, W.: The southwest Indian Monsoon over the last 18 000 year, Climate Dynamics, 12, 213–225, 1996.

Patterson, R. T., and Fishbein, E.: Re-examination of the statistical methods used to determine the number of point counts needed for micropaleontological quantitative research, J. Paleontol., 63(2), 245–248, 1984.

Pausata, F. S. R., Battusti, D. S., Nisancioglu, K. H. and Bitz, C. M.: Chinese stalagmite $\delta^{18}O$ controlled by changes in the Indian monsoon during a simulated Heinrich event, Nature Geoscience, 4, 474–480, 2011.

Peltier, W. R.: Global glacial isostasy and the surface of the ice-age earth: The ICE-5G (VM2) model and GRACE, Annual Review of Earth and Planetary Sciences, 32, 111–149, 2004.

Peterson, L. C., Haug, G. H., Hughen, K. A. and Röhl, U.: Rapid changes in the hydrologic cycle of the tropical Atlantic during the last Glacial, Science, 290, 1947–1951, 2000.

Peterson, L. C. and Huang, G. H.: Variability in mean latitude of the Atlantic Intertropical Convergence Zone as recorded by riverine input of sediments to the Cariaco Basin (Venezuela), Palaeogeography, Palaeoclimatology, Palaeoecology, 234, 97–113, 2006.

Phillips, S. C., Johnson, J. E., Giosan, L. and Rose, K.: Monsson-influenced variation in productivity and lithogenic sediment flux since 110 ka in the offshore Mahanadi Basin, northern Bay of Bengal, Marine and Petroleum Geology, 58, 502–525, 2014.

Prasad, T. G.: A comparison of mixed-layer dynamics between the Arabian Sea and Bay of Bengal: One-dimensional model results, Journal of Geophysical Research, 109, C03035, 2004.

Prasanna Kumar, S., Madhupratap, M., Dileep Kumar, M., Muraleedharan, P. M., de Souza, S. N., Gauns, M and Sarma, V. V. S. S.: High biological productivity in the central Arabian Sea during the summer monsoon driven by Ekman pumping and lateral advection, Current Science, 81, 1633–1638, 2001.

Prasanna Kumar, S., Muraleedharan, P. M., Prasad, T. G., Gauns, M., Ramaiah, N., de Souza, S. N., Sardesai, S. and Madhupratap, M.: Why is the Bay of Bengal less productive during summer monsoon compared to the Arabian Sea? Geophysical Research Letters, 29, 2235, 2002.

Prasanna Kumar, S., Narvekar, J., Nuncio, M. Ganus, M. and Sardesai, S.: What drives the biological productivity of the Northern Indian Ocean, Geophysical Monograph Series, 2009.

Randel, W. J. and Park, M.: Deep convective influence on the Asian summer monsoon anticyclone and associated tracer variability observed with Atmospheric Infrared Sounder (AIRS). J. Geophys. Res. Atmos., 111, D12314, 2006.

Rao, S. A., Saha, S. K., Pokhrel, S., Sundar, D., Dhakate, A. R., Mahapatra, S., Ali, S., Chaudhari, H. S., Shreeram, P., Vasimalla, S., Srikanth, A. S. and Suresh, R. R. V.: Modulation of SST, SSS over northern Bay of Bengal on ISO time scale, Journal of Geophysical Research, 116, C09026, 2011.

Rao, R. R. and Sivakumar, R.: Seasonal variability of sea surface salinity and salt budget of the mixed layer of the north Indian Ocean, Journal of Geophysical Research, 108, C13009, 2003.

Rashid, H., Flowe, B. P. Poore, R. Z. and Quinn, T. M.: A ~25ka Indian Ocean monsoon variability record from the Andaman Sea, Quaternary Science Reviews, 26, 2586–2597, 2007.

Schott, F.: Monsoon response of the Somali Current and associated upwelling, Progress in Oceanography, 12, 357–381, 1983.

Schott, F. A. and McCreary, J. P.: The monsoon circulation of the Indian Ocean, Progress in Oceanography, 51, 1–123, 2001.

Schulz, H., von Rad, U. and Erlenkeuser, H.: Correlation between Arabian Sea and Greenland climate oscillations of the past 110,000 years, Nature, 393, 54–57, 1998.

Sengupta, D., Bharath Raj, G. N. and Shenoi, S. S. C.: Surface freshwater from Bay of Bengal runoff and Indonesian Throughflow in the tropical Indian Ocean, Geophysical Research Letters, 33, L22609, 2006.

Shankar, D., Vinayachandran, P. N. and Unnikrishnan, A. S.: The monsoon currents in the north Indian Ocean, Progress in Oceanography, 52, 63–120, 2002.

Shenoi, S. S. C., Shankar, D., Shetye, S. R.: Differences in heat budgets of the near-surface Arabian Sea and Bay of Bengal: Implications for the summer monsoon, Journal of Geophysical Research, 107, C63052, 2002.

Shi, Y.: Characteristics of late Quaternary monsoonal glaciation on the Tibetan Plateau and in East Asia, Quaternary International, 97–98, 79–91, 2002.

https://doi.org/10.5194/cp-2020-27
Preprint. Discussion started: 6 March 2020

Shi, W, Morrison, J. M., Bryden, H. L.: Water, heat and freshwater flux out of northern Indian Ocean in September–October 1995, Deep-Sea Research II, 49, 1231–1252, 2002.

Sijinkumar, A. V., Clemens, S., Nath, B. N., Prell, W., Benshila, R. and Lengaigne, M.: $\delta^{18}O$ and salinity variability from the Last Glacial Maximum to Recent in the Bay of Bengal and Andaman Sea, Quaternary Science Reviews, 135, 79–91, 2016.

Sinha, A., Cannariato, K. G., Stott, L. D., Li, H.-C., You, C.-F., Cheng, H., Edwards, R. L. and Singh, I. B.: Variability of Southwest Indian summer monsoon precipitation during Bølling-Ållerød, Geology, 33, 813–816, 2005.

Singh, A. and Jani, R. A. and Ramesh, R.: Saptiotemporal variations of the $\delta^{18}O$-salinity relation in the northern Indian Ocean, Deep-Sea Research I, 57, 1422–1431, 2010.

Singh, A. D., Jung, S. J. A., Darling, K., Ganeshram, R., Ivanochko, T, and Kroon, D.: Productivity collapses in the Arabian Sea during glacial cold phases, Paleoceanography, 26, PA3210, 2011.

Sirocko, F., Garbe-Schönberg, D., McIntyre, A. and Molfino, B.: Teleconnections between the subtropical monsoons and high-latitude climates during the Last Deglaciation, Science, 272, 526–529, 1996.

Smith, R. D. and Gent, P. R.: Reference manual for the Parallel Ocean Program (POP), ocean component of the Community Climate System Model (CCSM2.0 and 3.0), Los Alamos National Laboratory, LAUR-02-2484, 2002.

Spiro Jaeger, G. and Mahadevan, A.: Submesoscale-selective compensation of fronts in a salinity-stratified ocean, Science Advance, 4, e1701504, 2018.

Stuiver, M. and Grootes, P. M.: GISP2 oxygen isotope ratios, Quaternary Research, 53, 277–284, 2000.

Stocker, T. F. and Johnsen, S. J.: A minimum thermodynamics model for the bipolar seesaw, Paleoceanography, 18, 1087, 2003.

Stoll H. M., Arevalos, A., Burke, A., Ziveri, P., Mortyn, G., Shimizu, N. and Unger, D.: Seasonal cycles in biogenic production and export in Northern Bay of Bengal sediments traps, Deep-Sea Research II, 54, 558–580, 2007.

Swingedouw, D., Mignot, J., Braconnot, P., Mosquet, E., Kageyama, M. and Alkama, R.: Impact of freshwater release in the North Atlantic under different climate conditions in an OAGCM, Journal of Climate, 22, 6377–6403, 2009.

Taylor, K. E., Stouffer, R. J. and Meehl, G. A.: An overview of CMIP5 and the experiment design, BAMS, 93, 485–498, 2012.

van de Poll, W. H., Kulk, G., Timmermans, K. R., Brussaard, C. P. D., van der Woerd, H. J., Kehoe, M. J., Mojica, K. D. A., Visser, R. J. W., Rozema, P. D. and Buma, A. G. J.: Phytoplankton chlorophyll α biomass, composition, and productivity along a temperature and stratification gradient in the northeast Atlantic Ocean, Biogeosciences, 10, 4227–4240, 2013.

Veldhuis, M. J. W.: Seasonal and spatial variability in phytoplankton biomass, productivity and growth in the northwestern Indian Ocean: the southwest and northeast monsoon, 1992–1993, Deep-Sea Research, 44, 425–449, 1997.

Vinayachandran, P. N., Murty, V. S. N., Ramesh Bahu, V.: Observations of barrier layer formation in the Bay of Bengal during summer monsoon, Journal of Geophysical Research, 107, 8018, 2002.

Wang, B., Clemens, S. C and Liu, P.: Contrasting the Indian and East Asian monsoons: implications on geologic timescales, Marine Geology, 201, 5–21, 2003.

Wang, X., Auler, A. S., Edwards, R. L., Cheng, H., Cristalli, P. S., Smart, P. L., Richards, D. A. and Shen, C.-C.: Wet periods in northeastern Brazil over the past 210 kyr linked to distant climate anomalies, Nature, 432, 740–743, 2004.

Webster, P. J., Magaña, V. O., Palmer, T. N., Shukla, J. Tmas, R. A., Yanai, M. and Yasunari, T.: Monsoons: Processes, predictability, and the prospects for prediction, Journal of Geophysical Research, 103, 14451–14510, 1998.

Wen, X., Liu, Z., Wang, S., Cheng, J. and Zhu, J.: Correlation and anti-correlation of the East Asian summer and winter monsoons during the last 21,000 years, Nature Communications, 7, 11999, 2016.

Wolff, E. W., Chappellaz, J., Blunier, T., Rasmussen, S. O. and Svensson, A.: Millennial-scale variability during the last glacial: The ice core record, Quaternary Science Reviews, 29, 2828–2838, 2010.

Yu, S.-Y., Colman, S. M. Lowell, T. V., Milne, G. A., Fisher, T. G., Breckenridge, A., Boyd, M. and Teller, J. T.: Freshwater ourbrust from Lake Superior as a trigger for the cold event 9300 years ago, Science, 328, 1262–1266, 2010.

Zhang, H., Liu, C., Jin, X., Shi, J., Zhao, S. and Jian, Z.: Dynamics of primary productivity in the northern South China Sea over the past 24,000 years, Geochemistry, Geophysics, Geosystems, 17, 4878–4891, 2016.

Zhang, R. and Delworth, T. L.: Simulated tropical response to a substantial weakening of the Atlantic thermohaline circulation, Journal of Climate, 18, 1853–1860, 2005.

Zhao, Y. and Harrison, S. P.: Mid-Holocene monsoons: a muti-model analysis of the inter-hemispheric differences in the responses to orbital forcing and ocean feedbacks, Climate Dynamics, 39, 1457–1487, 2012.

https://doi.org/10.5194/cp-2020-27
Preprint. Discussion started: 6 March 2020

Figures

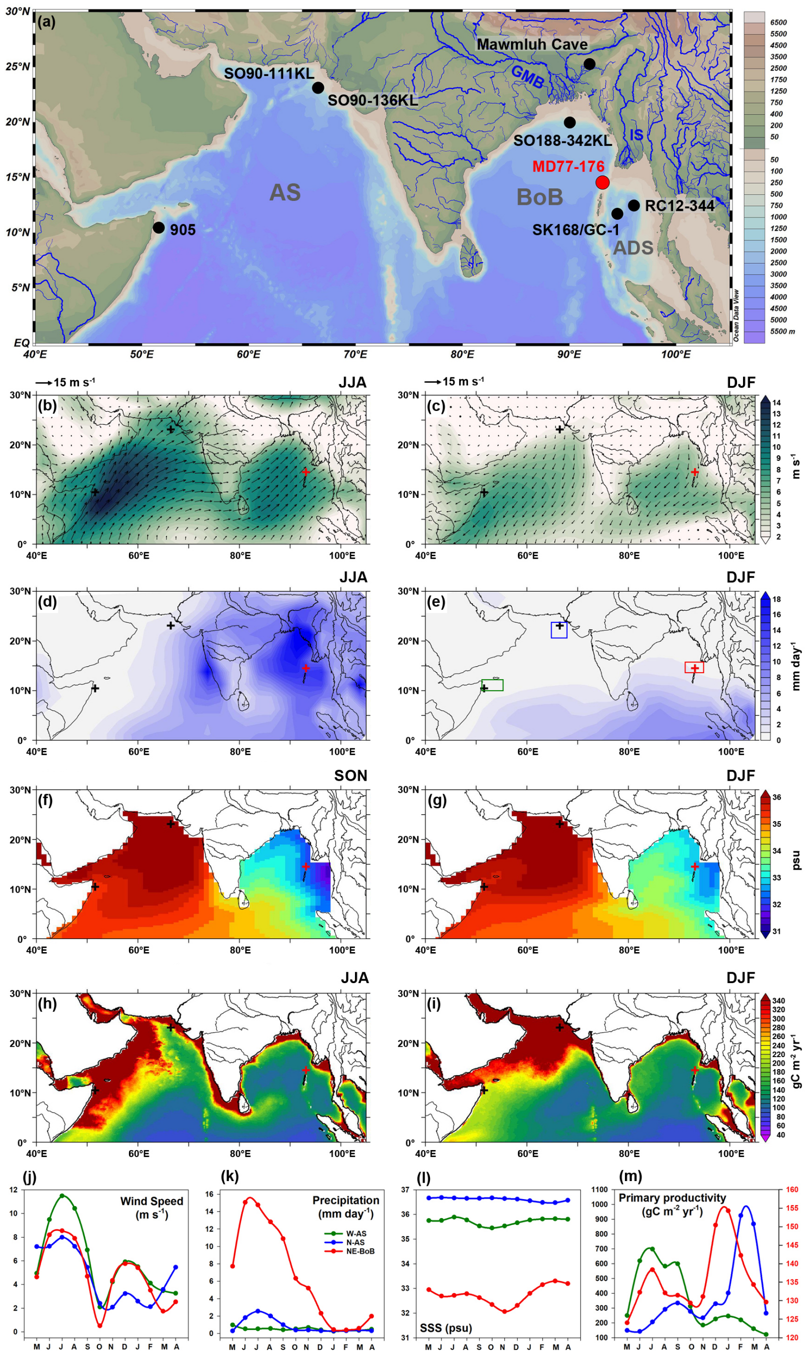

Fig. 1. (a) Geographic setting and bathymetric map of Indian Monsoon climate zone including the Arabian Sea (AS), the Bay of Bengal (BoB) and the Andaman Sea (ADS). The map was created by the Ocean Data View software (©Reiner Schlitzer, Alfred Wegener Institute) with its built-in global high resolution bathymetric data (GlobHR). Location of the sediment core of the current study is marked by the red circle. Black circles mark the location of published records shown in Fig. 4. (b) and (c) Mean (from 1979 to 2018) surface wind speed and wind vectors for north hemisphere (NH) summer (June, July, August, JJA) and winter (December, January, February, DJF), respectively. Data is from NCEP-DOE Reanalysis 2 (http:// esrl.noaa.bov/psd/data/grided/data.ncep.reanalysis2.html). (d) and (e) Mean (from 1979 to 2018) precipitation rate for NH winter and summer respectively. Data is from CPC Merged Analysis of Precipitation (http:// esrl.noaa.bov/psd/data/grided/data.ncep.camp.html). (f) and (g) Mean (from 1979 to 2018) surface seawater salinity (SSS) for NH autumn (September, October, November, SON) and winter respectively. Data is from NCEP Global Ocean Data Assimilation System (http:// esrl.noaa.bov/psd/data/grided/data.godas.html). (h) and (i) Mean (from 2003 to 2018) net primary productivity for NH summer and winter respectively. PP data is based on MODIS chlorophyll-a and calculated using the VGPM model (http:// science.oregonstate.edu/ocean.productivity). (j), (k), (l) and (m) Regional climatology and oceanography in the western AS, northern AS and northeastern BoB. The selected regions are marked by color rectangles in (e). Data sources are the same with above.

https://doi.org/10.5194/cp-2020-27
Preprint. Discussion started: 6 March 2020

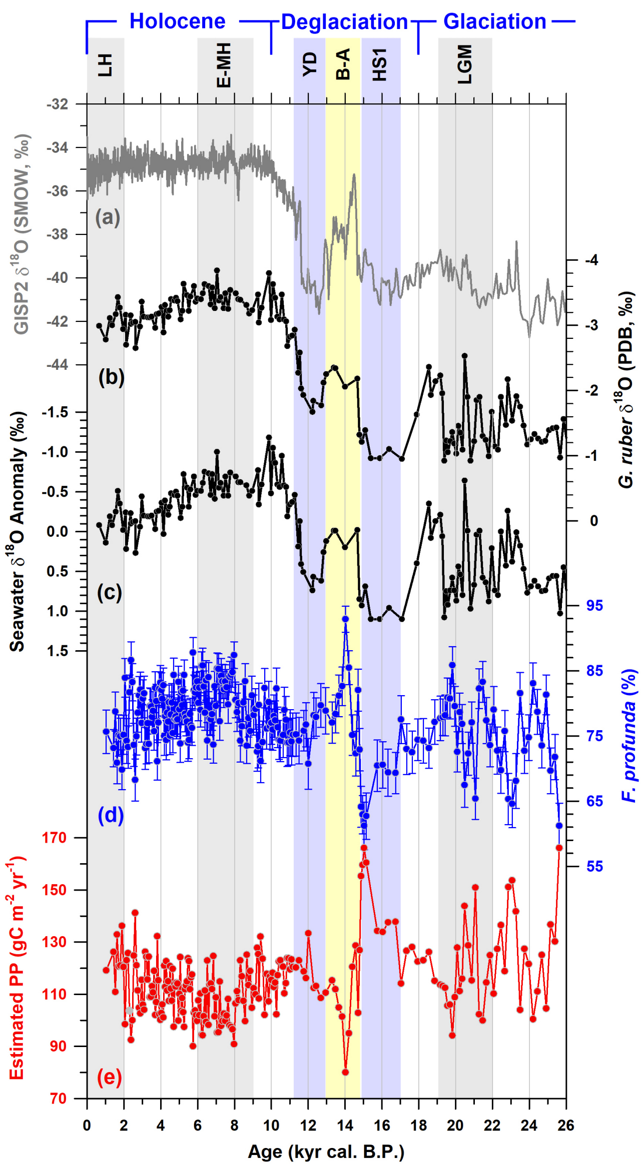

710 **Fig. 2.** (a) GISP2 Greenland ice core $\delta^{18}O$ signal (Stuiver and Grootes, 2000). (b) *Globigerinoides ruber* $\delta^{18}O$ record of core MD77-176 (Marzin et al., 2013). (c) Seawater $\delta^{18}O$ anomaly obtained on core MD77-176 (Marzin et al., 2013). (d) *F. profunda* relative abundance (Fp%) of core MD77-176 (this study). The error bars mark the 95% intervals. (e) Primary productivity calculated by MD77-176 Fp% using the tropical Indian Ocean empirical equation (Hernández-Almeida et al., 2019).

https://doi.org/10.5194/cp-2020-27
Preprint. Discussion started: 6 March 2020

715

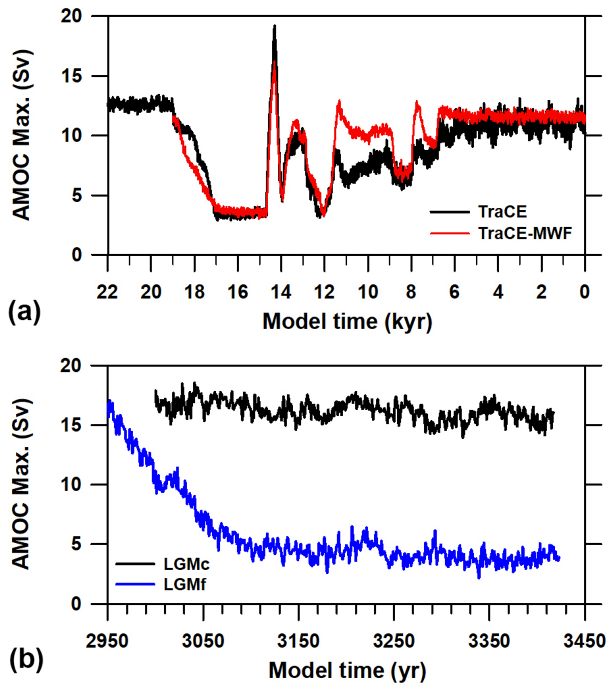

Fig. 3. The changes of the maximum in the AMOC streamfunction below 500 m (AMOC strength) in (a) TraCE and TraCE-MWF experiments, and in (b) LGMc and LGMf experiments run with IPSL-CM5A-LR.

https://doi.org/10.5194/cp-2020-27
Preprint. Discussion started: 6 March 2020

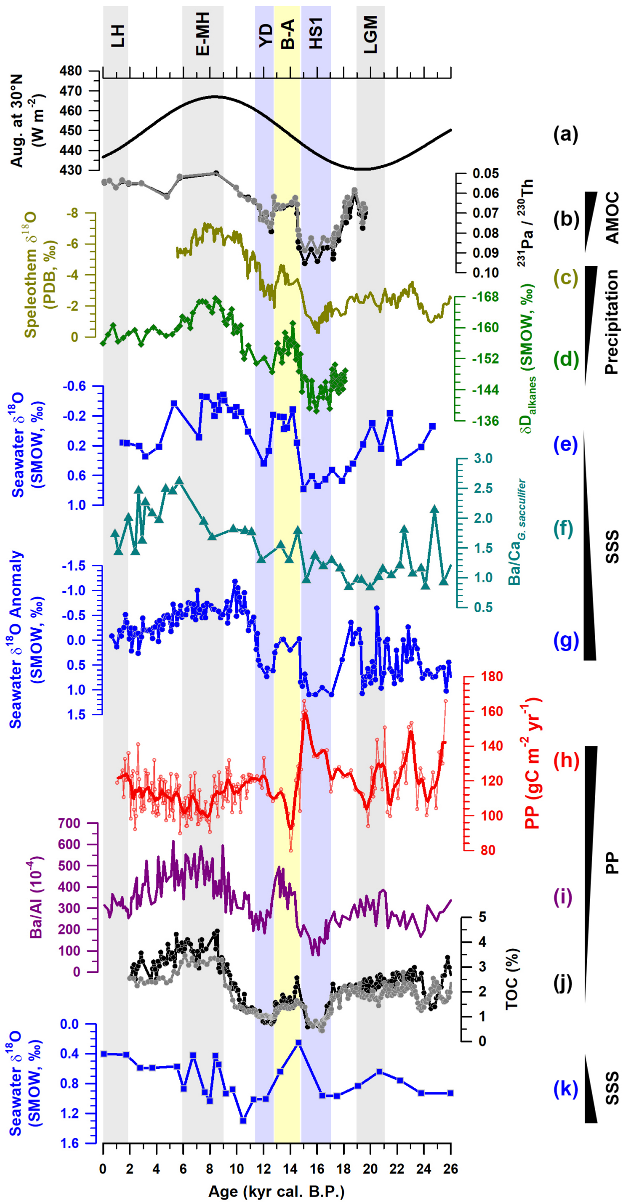

Fig. 4. (a) August mean insolation at 30°N. (b) AMOC strength indicated by $^{231}Pa/^{230}Th$ ratio of marine sediment from the western subtropical Atlantic Ocean (McManus et al., 2004). (c) Mawmluh Cave speleothem δ^{18}O (Dutt et al., 2015). (d) Alkane δD in marine sediment, core SO188-342 (Contreras-Rosales et al., 2016). (e) Seawater δ^{18}O record of core RC12-344 (Rashid et al., 2007). (f) Ba/Ca ratios derived from mixed layer foraminifer species *Globigerinoides sacculifer* from core SK 168/GC-1(Gebregiogis et al., 2016). (g) Seawater δ^{18}O anomaly record

https://doi.org/10.5194/cp-2020-27
Preprint. Discussion started: 6 March 2020

Climate of the Past Discussions

of core MD77-176 (Marzin et al., 2013). (h) Estimated PP record of core MD77-176 (this study). The thick red curve shows the result of a 500-year smoothing. (i) Ba/Al ratio of marine sediment, core 905 (Ivanochko et al., 2005). (j) Total organic carbon weight percentage of marine sediment, core SO90-111KL (gray) and SO90-136KL (black) (Schulz et al., 1998). (k) Seawater $\delta^{18}O$ record of core 905 (Anand et al., 2008). Core locations of all these records above are marked in Fig. 1a.

https://doi.org/10.5194/cp-2020-27
Preprint. Discussion started: 6 March 2020

Climate of the Past
Discussions

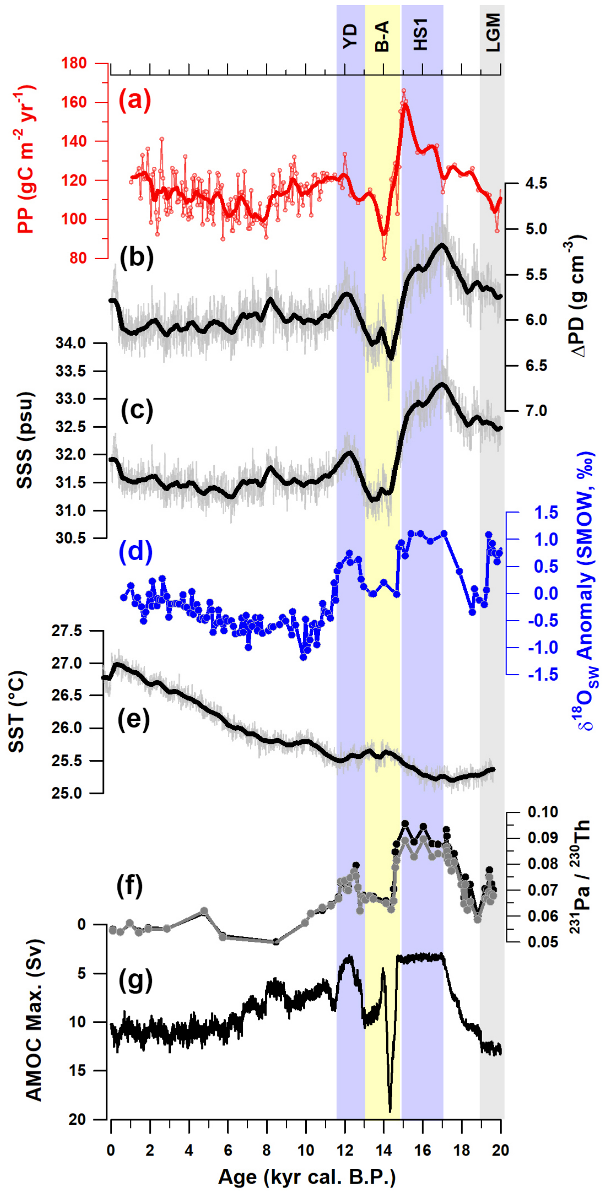

730 **Fig. 5.** (a) Estimated-PP of core MD77-176 (this study). (b), (c), (e) and (g) are the results of the TraCE-21 simulation outputs of oceanic parameters in the northeastern BoB (the data grids are marked in Fig. S7). (b) Annual mean potential density difference between 200 and 5 m water depth (ΔPD). (c) Annual mean SSS (5m); (d) Seawater $\delta^{18}O$ anomaly record of core MD77-176 (Marzin et al., 2013). (e) Annual mean SST (5m). (f) AMOC

https://doi.org/10.5194/cp-2020-27
Preprint. Discussion started: 6 March 2020

strength indicated by $^{231}Pa/^{230}Th$ ratio of marine sediment from the western subtropical Atlantic Ocean (McManus et al., 2004). (g) Maximum flux of the AMOC in the TraCE-21 simulation.

https://doi.org/10.5194/cp-2020-27
Preprint. Discussion started: 6 March 2020

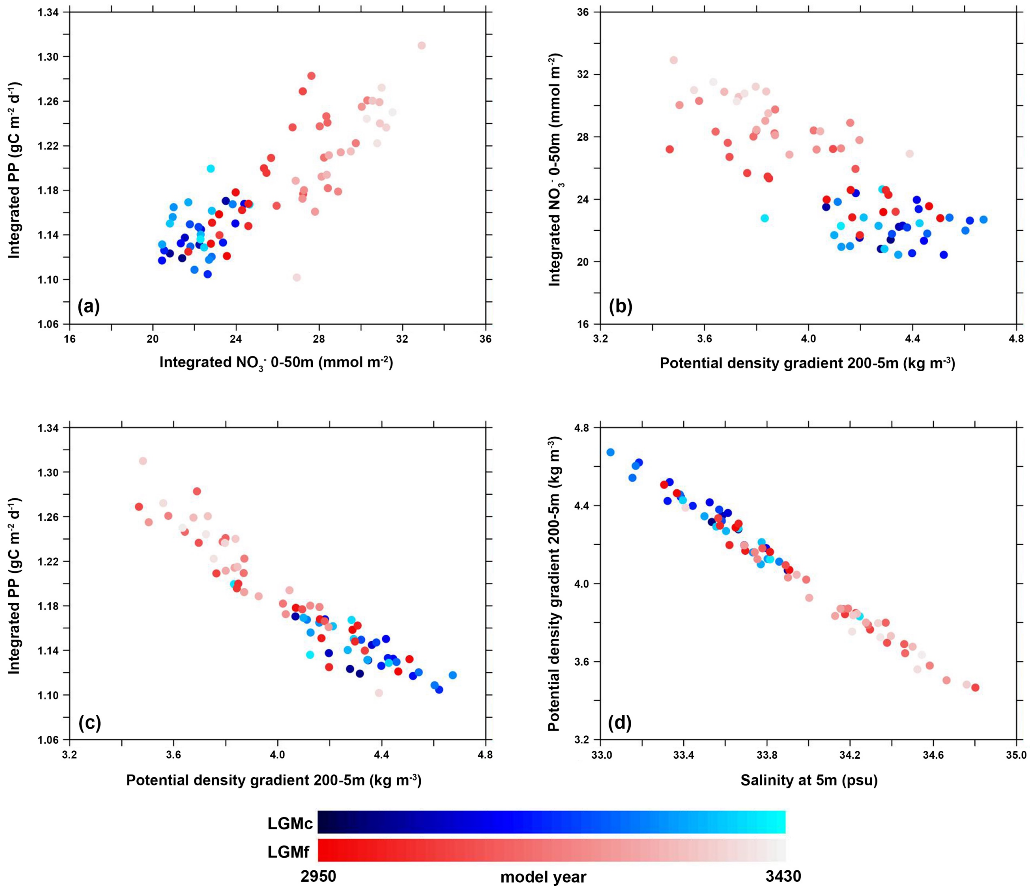

Fig. 6. Correlations between different oceanic parameters computed with the IPSL-CM5-LR model in experiments LGMc and LGMf for the northern BoB (the data grids are marked in Fig. S7). The results are DJF mean and every dot represents an average of ten model years (section 3.3; Fig. 3b). (a) Integrated nitrate content of the upper 50 m vs integrated PP of the whole seawater column. (b) Potential density difference between 200 and 5 m vs integrated nitrate content of the upper 50 m. (c) Potential density difference between 200 and 5 m vs integrated PP of the whole seawater column. (d) Salinity at 5 m vs potential density difference between 200 and 5 m seawater.

https://doi.org/10.5194/cp-2020-27
Preprint. Discussion started: 6 March 2020

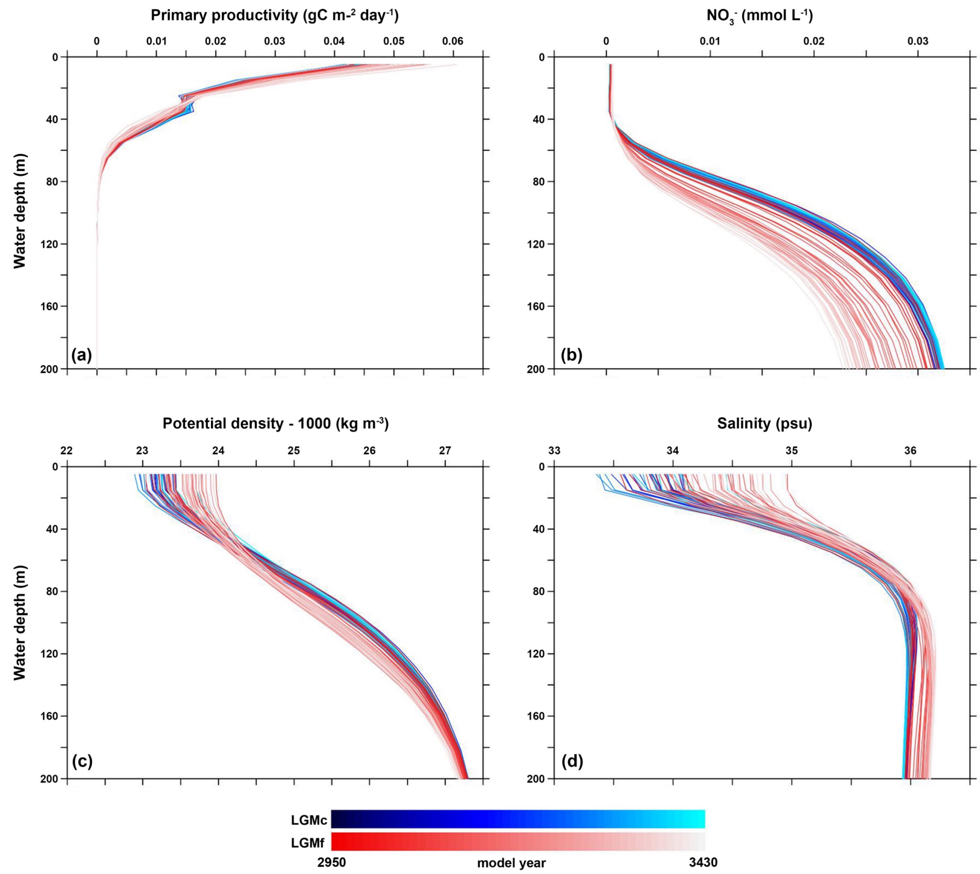

Fig. 7. Vertical profiles of oceanic parameters of the IPSL-CM5-LR experiments LGMc and LGMf in the northern BoB (the data grids are marked in Fig. S7). The results are DJF mean and every curve represents an average of ten model years (section 3.3; Fig. 3b). (a) Primary productivity. (b) Nitrate concentration. (c) Potential density. (d) Salinity.

https://doi.org/10.5194/cp-2020-27
Preprint. Discussion started: 6 March 2020

Climate of the Past
Discussions

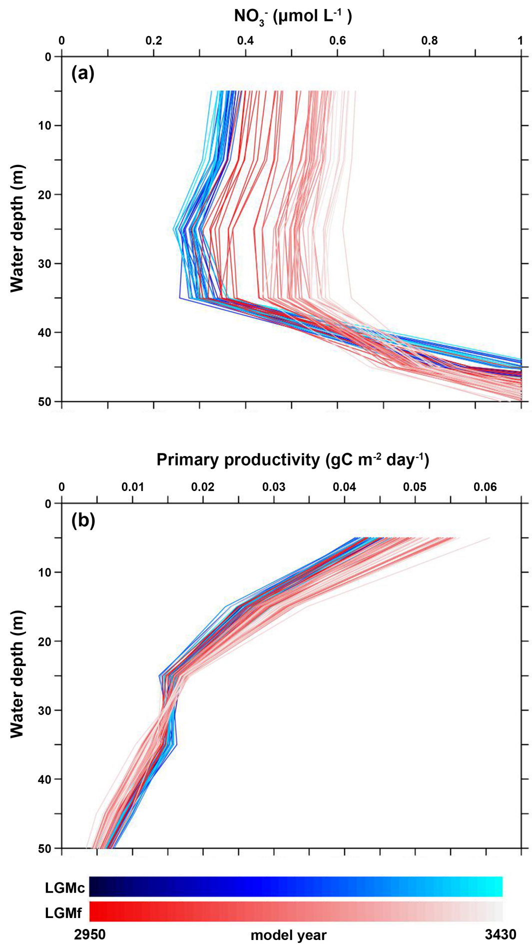

Fig. 8. Vertical profiles of oceanic parameters of the IPSL-CM5-LR experiments LGMc and LGMf in the northern BoB (the data grids are marked in Fig. S7). The results are DJF mean and every curve represents an average of 10 model years (section 3.3; Fig. 3b). (a) Nitrate concentration. (b) Primary productivity.